DESIGN METHODOLOGY FOR THE CONTROL OF PLANAR TRANSFORMER PARASITICS

SAMUEL R. COVE

Design Methodology for the Control of Planar Transformer Parasitics

by

© Samuel R. Cove

A thesis submitted to the
School of Graduate Studies
in partial fulfilment of the
requirements for the degree of
Master of Engineering

Faculty of Engineering and Applied Science
Memorial University of Newfoundland

March 2011

St. John's Newfoundland

Abstract

Planar transformers provide a light-weight and low profile solution for power electronic converters with highly reproducible parameters and simple manufacturability. Parasitic inductances, capacitances, and resistances in planar magnetics are difficult to model due to the complex interactions between the physical winding arrangement of each layer and the core geometry (track width, air gap, clearance, etc.). These nonlinear and multivariate magnetic devices play a key role in defining the performance of traditional, soft-switching, and resonant converters by ruling behaviors such as ringing, self-resonant frequency, conduction losses, and current rate of change in these converters. In this work, a methodology for determining parametric models for leakage and magnetizing inductance, inter and intra-winding capacitances, and winding resistance of small planar transformers is presented using a variety of winding arrangements.

First, finite element analysis is investigated for the extraction of planar transformer parasitics from 3D designs. Then a Central Composite Design based on the Design of Experiment (DoE) methodology is employed on finite element simulations to provide comprehensive parasitic models based on winding geometry. Results from physical verification on a planar ER18/3.2/10 core set are provided and show excellent correlation between models and verification tests. The method is later employed to effectively design an LLC (inductor-inductor-capacitor) resonant converter, which is also experimentally verified to illustrate the benefits of the proposed method. The methodology can be employed to characterize and design planar transformers and to predict their performances as part of a variety of power electronic converters.

Acknowledgements

I would like to express my sincere gratitude to my primary supervisor Dr. Martin Ordonez for providing me with the exciting opportunity to be a part of his team. I would like to thank him for his outstanding teaching, extreme dedication and moral support throughout my Master's research. I am also very grateful to have had Dr. John Quaicoe as my co-supervisor. His exceptional advice, guidance and support have been invaluable to my research and my future goals.

I would like to acknowledge my colleague Federico Luchino for his assistance with the experimental results presented in this work. His knowledge of printed circuit board design, DC-DC converter design, digital signal processing, and experimental testing procedures were crucial to the timely completion of my research. Special thanks to my colleagues Lucas Sinopoli and Juan Galvez for their assistance and support.

I would like to thank Memorial University of Newfoundland, the Natural Sciences and Engineering Research Council of Canada (NSERC) and the Industrial Research and Innovation Fund (IRIF) for funding this research. I wish to acknowledge Ansoft Corporation for providing in-kind discounts for the software license required to run finite element simulations and Sunstone Circuits for their design assistance and fabrication of the printed circuit boards used for experimental testing.

Finally, I owe my deepest gratitude to my fiancée Deanne Drover and my parents Sam and Agnes Cove for their patience, understanding and moral support through the long days and nights spent working on my research.

Contents

List of Tables

List of Figures

Chapter 1

Introduction

1.1 Planar Transformers

Frequently the bulkiest, heaviest, and most costly components with the greatest effect on the performance of power electronic systems are the magnetic components: the inductors and transformers. Ongoing research to reduce the size and weight of these components is gaining interest through the investigation of high frequency planar magnetics [1, 2, 3, 4]. Planar transformers use ferrite cores which have a lower profile and a larger footprint. The windings are made of copper shims, stamps, or printed circuit board traces with thicknesses much smaller than their widths. This is very different from the traditional wire-wound transformers which use wire with circular cross-sections in cores whose footprint is much smaller than their profile. Figure 1.1 highlights the dimensional differences between planar and wire-wound transformer cross-sections.

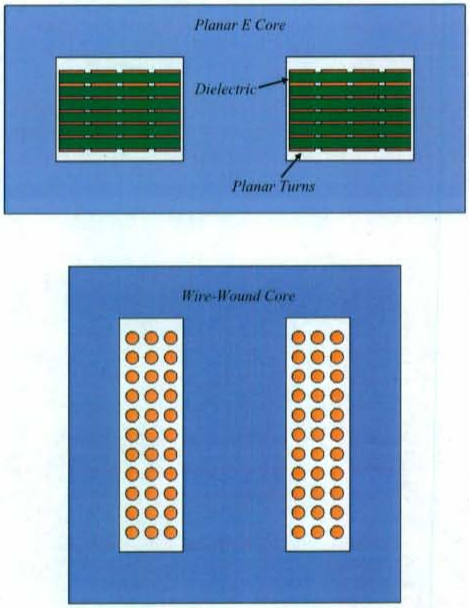

Figure 1.1: Cross-sections of planar and wire-wound transformers

1.1.1 Planar Transformer Advantages

Planar transformers provide a number of benefits over their wire-wound counterparts [5, 6, 7, 8]. The main benefits are:

1. Increased thermal management. The low-profile high-footprint design of planar cores provides a larger surface area to mount heatsinks which allows higher power densities to be realized.

2. Low leakage inductance. The planar design allows for less flux to escape between the copper windings and it is easier to interleave windings in planar transformers to further decrease the leakage inductance.

3. Lower high frequency losses. The planar winding structure allows for designs with thicknesses of two skin depths to reduce skin effect losses at high frequencies. The large width of the conductor increases the current capacity of the winding.

4. High reproducibility. When built into printed circuit boards the windings of planar transformers are highly manufacturable and can be recreated with negligible error. This allows for exact replicas to be modeled using finite element software and for the prediction of the transformer non-idealities (referred to as parasitics) to a high degree of accuracy. Wire-wound transformers cannot be reliably wound the exact same way so any prediction of this sort would be difficult.

This work's primary focus is employing the high reproducibility of printed circuit board planar transformers to develop a method to model their parasitic levels over a

wide range of winding design parameters.

1.1.2 Planar Transformer Parasitic Effects

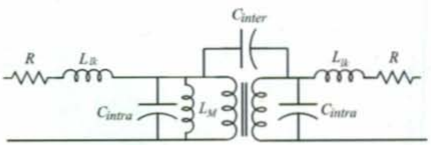

Figure 1.2: High frequency planar transformer equivalent circuit

The winding design of planar transformers is a challenging trade off process in which the winding structure affects the transformer's electromagnetic, thermal, power flow, and parasitic behaviour simultaneously. Figure 1.2 contains the equivalent circuit of a planar transformer which highlights the parasitic elements of interest in this thesis: magnetizing inductance (L_M), leakage inductance (L_{lk}), inter-winding capacitance (C_{inter}), intra-winding capacitance (C_{intra}), and winding resistance (R).

L_M is a measure of the magnetic coupling between the primary and the secondary of the transformer. It is a measure of the amount of magnetic flux which entirely encompasses the primary and the secondary windings. L_{lk} represents the magnetic energy which does not transfer from the primary to the secondary. It is a measure of the magnetic flux which only encompasses either the primary or the secondary winding. C_{inter} represents the charge storage capability of the dielectric material between the two windings. It is a measure of the capability of the transformer to transfer transient voltage spikes from the primary to the secondary directly, bypassing the magnetic coupling. C_{intra} represents the charge storage capability of the dielectric

between each turn or layer of each winding. R is the winding copper resistance which represents the ohmic losses of each winding.

1.2 Transformers Parasitics in DC-DC Converters

Transformer parasitics play a critical role in the operation of a variety of DC-DC converter topologies and need to be controlled for this reason. Now that the equivalent circuit and parasitic descriptions have been established, the requirements on each parasitic to help achieve higher efficiency and increased power density in traditional, zero voltage switching, and resonant converter topologies are described in this section.

1.2.1 Traditional DC-DC Converters

Transformers are important in traditional hard-switching DC-DC converters for two reasons: to provide electrical isolation to the electronics downstream from the converter and to assist in achieving high or low voltage gains by stepping up or down the input voltage. In both of these applications each parasitic level must be at a minimum to decrease energy losses in the transformer and to avoid constraints on di/dt and voltage ringing at the secondary of the transformer. Figure 1.3 highlights the di/dt on the primary current of the transformer caused by L_{lk} and the voltage ringing at the secondary caused by the second order characteristic of the interaction between L_{lk} and C_{intra}. The parasitics have a profound impact on the overshoot (Vs_{peak}), the ringing frequency (f), and the di/dt in traditional DC-DC converter topologies and must be minimized.

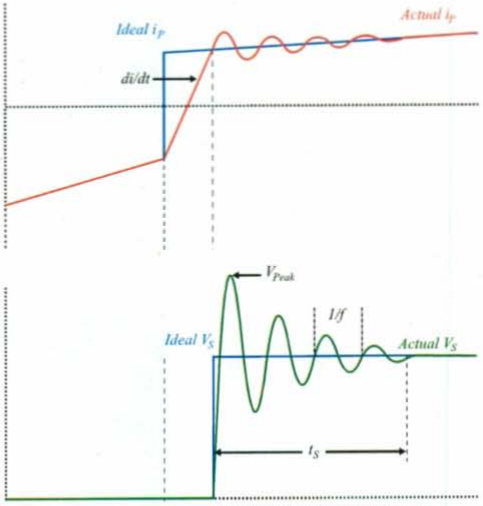

Figure 1.3: Conceptual transformer secondary voltage and current in a traditional DC-DC converter with parasitic ringing and di/dt constraint

1.2.2 Zero Voltage Switching Converters

Transformer parasitics play an integral part in soft-switching converter topologies. In phase-shift Zero Voltage Switching (ZVS) operation, the energy from the leakage inductance is used to force a zero voltage state before the converter switches turn on, minimizing switching losses associated with each switch output capacitance [9, 10, 11, 12]. This allows for higher frequency operation which reduces the size of the transformer. The most important requirement for ZVS operation is that the leakage inductance be able to store more energy than the output capacitance of each switch. The challenge is to design a transformer winding which contains a predefined level of L_{lk} while minimizing the effects from other parasitics.

1.2.3 Resonant Converters

Resonant converters require passive electromagnetic structures (inductors and capacitors) to create resonance in the circuit which varies the gain of the converter based on the switching frequency [13, 14]. LLC resonant converters are gaining popularity due to their soft switching characteristics which are very important to reducing losses [15, 16, 17, 18, 19]. The resonance in an LLC resonant converter is dependent on a capacitor and inductor in series with a parallel inductance. The series inductor can be replaced by the transformer leakage inductance and the parallel inductor can be replaced by the magnetizing inductance when using the transformer as an integrated magnetic component. The resonant frequencies, the gain characteristics, and the region of operation are highly reliant on the precise value of L_{lk} and L_M so when designing a planar transformer for an LLC resonant converter, L_{lk} and L_M are

designed to specific values while the remaining parasitics are to be minimized. This is a significant challenge that is addressed by the methodology proposed in this thesis.

1.3 Modeling of Planar Transformers

The previous section established the importance of controlling the parasitics. This section investigates the use of a combination of finite element modeling (FEM) and design of experiment methodology (DoE) for developing high accuracy parasitic prediction models. FEM is very important when designing magnetics to observe the electromagnetic field distributions and measure parasitic levels without requiring expensive and time-consuming fabrication. DoE is an efficient statistical methodology for creating parametric models from empirical data gathered from FEM simulations or experimental testing. Combining FEM and DoE methodology creates a powerful tool for predicting parasitic levels in planar transformers over a wide range of winding design parameters.

1.3.1 Finite Element Modeling of Planar Transformers

Electromagnetic FEM simulations break the simulations space into small tetrahedrons which make up the finite element mesh. The electromagnetic field quantities are solved at each node of the mesh and are interpolated elsewhere. The mesh can be made fine or coarse, where fine meshes improve accuracy but also increase simulation time, while a coarse mesh will provide a rough approximation for rapid prototyping. In Chapter 2 FEM is investigated for the calculation of planar transformer parasitics. The equations and background theory are presented along with methods for calculat-

ing each parasitic. The chapter concludes with a design example which confirms the high accuracy of the proposed methods.

1.3.2 Modeling Parasitic Behavior

While FEM is an exceptional tool for modeling the parasitic effects in planar transformers, it can only be applied to discrete values of winding design parameters. To create continuous functions for each transformer parasitic based on complex winding design parameters, DoE methodology is employed in conjunction with FEM. DoE provides a statistical method for defining parametric models for planar transformer parasitics with a minimum of experiments while maintaining a high level of accuracy [20]. In Chapter 3 DoE is used to create parametric models for each parasitic with respect to the following winding design parameters: track width ratio, air gap length, conductor clearance, and number of turns per winding. Very high accuracy quadratic models are presented using twenty-five FEM simulations which predict the parasitic levels over a wide range of winding design parameters. In Chapter 4 a design procedure is provided to use these models to design a transformer with specific levels of magnetizing and leakage inductance for an LLC resonant converter. The design accounts for the need for minimum resistive and capacitive parasitics and is experimentally confirmed to operate as designed.

1.4 Current Literature and Proposed Research

The previous sections outline the scope of this work: to create a methodology for the accurate prediction of planar transformer parasitics to use for transformer design

in various DC-DC converter topologies. This section positions this goal in the context of current work in the areas of parasitic prediction and the application of DoE methodology to magnetics.

Currently analytical models are available for transformer leakage inductance, capacitance, and losses using conventional winding arrangements and approximations [21, 22, 23, 24, 25, 26, 27, 28]. Modeling leakage inductance under conventional winding arrangements with the assumption of symmetry and linear MMF distribution has been addressed [21, 22]. Aspects relating to power losses have been addressed by an interesting approach to vary track-width to minimize resistance [23], an analytical solution which is accurate for transformers with fixed-width conductor without gapped core [24], and models for loss and heat rise calculations based on analytical and empirical formulae [25]. Other individual parameters such as capacitances have been studied in wire-wound transformers, including a method for calculating self capacitance [26], methodology based on a two-port network and step response to model stray capacitances [27], and the use of inter-winding capacitance to achieve ZVS and Zero-Current Switching (ZCS) [28]. Investigations of the previous important effects in Printed Circuit Board (PCB) based planar transformers are lacking in the literature, and comprehensive modeling methods that combine interactions of physical parameters in non-traditional winding arrangements have not been addressed either.

Preliminary work on applying Design of Experiment methodology to electromagnetics has been performed [29, 30, 31, 32]. Response Surface Methodology has been applied to the design of a C-core actuator [29], magnetic levitation systems [30], high temperature superconducting transformers [31], and E-core planar transformers [32]. The existing literature provides a solid basis for the use of this technique to analyze

the effect of complex winding design parameters in small planar transformer design, which has not previously been examined.

This work addresses the technical challenges outlined above by modeling and characterizing parasitics in more complex geometries, and providing a useful methodology to accurately control parasitics during planar transformer design stages. The systematic experimental methodology covered in this thesis contributes to the field of planar magnetic design, modeling, and characterization by:

1. Providing a fast, efficient, and accurate approach to the prediction of parasitics in planar transformers, which control undesired effects such as voltage ringing and restrictions on di/dt.

2. Addressing planar parasitics comprehensively, by using complex winding design parameters without the use of assumptions.

3. Investigating the effect of varying turn track widths on all parasitics, a novel contribution to transformer winding design methods with applications in integrated magnetics.

4. Creating an effective design procedure to select the appropriate transformer parasitics for LLC resonant converters.

5. Providing highly accurate experimental verification of results.

Chapter 2

Finite Element Modeling of High Frequency Planar Transformers

2.1 Introduction

Planar transformer parasitics are highly complex and nonlinear, especially when using complex winding geometries. Analytical solutions require simplifications and assumptions of symmetry which are not present in physical transformers. Due to high precision manufacturing and increased reproducibility, high frequency planar transformers built into printed circuit boards offer the ability to model their parasitics with high accuracy using finite element simulations which require less assumptions and no symmetry[33].

Finite element simulations segment the simulation space into small tetrahedrons called a mesh and solve Maxwell's equations at every mesh node and at every edge midpoint to simulate the electromagnetic field parameters inside the simulation. A

quadratic interpolation function is used to calculate the values of the electromagnetic field parameters between nodes. It is a conscious decision to make the mesh as fine or as coarse as is necessary to balance the accuracy of the model with runtime speed. In the following sections the theory behind the simulation of inductance, resistance, and capacitance within finite element models is described and the procedures to calculate parasitic values within high frequency planar transformers are defined. A design example is included to highlight the effectiveness and accuracy of the procedures with regards to modeling planar transformer parasitics.

2.2 Simulating Circuit Parameters

Finite element simulations are performed using various solvers which calculate a subset of the field parameters to save computing time. The three steady state solvers (electrostatic, magnetostatic, and eddy current solvers) are used to model the parasitic effects in high frequency planar transformers. The electrostatic solver is used to calculate capacitance, the magnetostatic solver is used to calculate DC resistance and inductance, and the eddy current solver is used to measure AC resistance and inductance. The background theory and methodology for calculating these circuit parameters are presented in the following sections.

2.2.1 Simulating Capacitance

Measuring capacitance in finite element simulations requires the use of the electrostatic solver, which assumes there is no movement of charge within the simulation space and all conductors are treated as perfect conductors in electrostatic equilibrium.

Electrostatic simulations can be excited using a charge density (ρ) which is used to compute the electric potential (Φ) at every node of the simulation mesh using the equation:

$$\nabla \cdot (\epsilon_r \epsilon_0 \nabla \Phi) = -\rho \tag{2.1}$$

which is derived from Gauss's Law (2.2), the electric field constitutive relation (2.3), and the definition of the electric potential (2.4):

$$\nabla \cdot \vec{D} = \rho \tag{2.2}$$

$$\vec{D} = \epsilon \vec{E} \tag{2.3}$$

$$\vec{E} = -\nabla \Phi \tag{2.4}$$

where ϵ_r and ϵ_0 represent the relative and free space permittivities, $\vec{D}$ represents the electric flux density, and $\vec{E}$ represents the electric field intensity.

Electrostatic simulations are used to calculate capacitance (C) within high frequency planar transformers using the electric potential energy (U_E) which is defined over the volume (V) of the simulation domain using (2.5) and (2.6):

$$U_E = \frac{1}{2} \int_V \vec{E} \cdot \vec{D} \, dV \tag{2.5}$$

$$U_E = \frac{1}{2} C V^2 \tag{2.6}$$

Solving the two equations for the capacitance gives:

$$C = \frac{1}{V^2} \int_V \vec{E} \cdot \vec{D} \, dV \tag{2.7}$$

To further simplify the modeling, when calculating capacitances using the electrostatic solver, (2.7) can simplify to twice the energy defined in (2.5) when the transformer is excited with $V = 1V$. Using this method it is quick and easy to determine the capacitance by summing the values of the electrostatic energy calculated at every node of the mesh.

2.2.2 Simulating DC Resistance and Inductance

To model DC inductance and resistance in finite element simulations the magnetostatic solver is used, which assumes that only DC currents can flow and there can be no time-varying magnetic fields. The conductors are treated as non-ideal and thus electric fields are allowed to penetrate them. Any currents induced in the simulation must be divergenceless, meaning that the current must either be fully contained within the boundaries of the simulation or any current that enters the simulation boundaries must also exit the boundaries as well. Magnetostatic solutions can be excited by external voltages (V), current (I), current density ($\vec{J}$), or permanent magnetizations ($\vec{M}$). The solver performs two solutions sequentially: first the current density in all conductors is determined, then the magnetic field quantities are computed. The current densities are determined by first solving for the electric potential (Φ) within the conductor using:

$$\vec{J} = \sigma \vec{E} \tag{2.8}$$

When (2.8) is combined with (2.4), the field solution becomes:

$$\vec{J} = -\sigma \nabla \Phi \tag{2.9}$$

Considering the field is magnetostatic, the final field constraint is that the continuity equation must be preserved:

$$\nabla \cdot \vec{J} = \frac{\partial \rho}{\partial t} = 0 \tag{2.10}$$

Combining (2.9) and (2.10) allows for the electric potential to be calculated using:

$$\nabla \cdot (\sigma \nabla \Phi) = 0 \tag{2.11}$$

This equation is solved at every node in the simulation and the current density is derived from the solution using (2.9).

Once the current density has been solved, the magnetostatic solver computes the magnetic field intensity ($\vec{H}$) and the flux density ($\vec{B}$) from Ampères circuital law and Gauss's law for magnetism:

$$\nabla \times \vec{H} = \vec{J} \tag{2.12}$$

$$\nabla \cdot \vec{B} = 0 \tag{2.13}$$

using the magnetic constitutive relationship:

$$\vec{B} = \mu(\vec{H} + \vec{M}) \tag{2.14}$$

where $\vec{M}$ represents any permanent magnet excitation within the solution region.

These field quantities are important to solve for inductance (L) within high frequency planar transformers through the magnetic energy (U_M):

$$U_M = \frac{1}{2} \int_V \vec{B} \cdot \vec{H} \, dV = \frac{1}{2} L I^2 \tag{2.15}$$

Solving this equation for the inductance (L) gives:

$$L = \frac{1}{I^2} \int_V \vec{B} \cdot \vec{H} \, dV \tag{2.16}$$

To solve for inductances within high frequency planar transformers, the winding is excited with $I = 1A$ which allows the magnetic energy to represent the inductance of the transformer.

2.2.3 Simulating AC Resistance and Inductance

The eddy current solver allows for time varying excitations and electromagnetic field solutions to solve for AC resistance and inductance values. This solver incorporates the skin depth and it simplifies the solution of the electromagnetic field quantities by assuming they all pulsate at the same frequency and stores the values in phasor format. The excitations for this solver must be a phasor current or current density. Similar to the magnetostatic solver, the eddy current solver solves for magnetic fields inside conductors before solving the fields elsewhere. The current density is calculated using the phasor forms of the equations found in the magnetostatic solution, while the magnetic field intensity is calculated inside the conductors using Ampères Circuital Law in phasor form:

$$\nabla \times \vec{H} = \vec{J} + j\omega\epsilon\vec{E} \tag{2.17}$$

and using (2.8) in phasor form along with Faraday's Law:

$$\nabla \times \vec{E} = -j\omega\vec{B} \tag{2.18}$$

provides the field equation in phasor form:

$$\nabla \times (\frac{1}{\sigma + j\omega\epsilon} \nabla \times \vec{H}) = j\omega\mu\vec{H} \tag{2.19}$$

This equation is used to compute the magnetic field intensity at every node in the mesh in phasor form. The simulation can be iterated through numerous frequencies to provide harmonic analysis of the magnetic field quantities. The inductance can be calculated at any frequency using the phasor expression of (2.16):

$$L = \frac{1}{I^2} \int_V \vec{B} \cdot \vec{H}^* \, dV \tag{2.20}$$

while the AC resistance can be calculated using the ohmic power losses (P):

$$P = \int_V \frac{\vec{J} \cdot \vec{J}^*}{2\sigma} \, dV = \frac{1}{2} I^2 R \tag{2.21}$$

$$R = \frac{1}{\sigma I^2} \int_V \vec{J} \cdot \vec{J}^* \, dV \tag{2.22}$$

To determine the inductance and resistance at any harmonic frequency in a high frequency planar transformer an eddy current model is solved with current $I = 1A$ and the magnetic and loss energy are used to represent the inductance and resistance respectively.

2.3 Design Example: High Frequency Planar Transformer

To demonstrate the ability of finite element analysis to accurately portray parasitics in high frequency planar transformers a design example is presented. The transformer

is built into a standard four layer printed circuit board using an ER18/3.6/10 core set with construction parameters as established in Table 2.1. Two layers were used for primary and two layers were used for secondary. As a proof of concept the transformer is an isolation transformer with a turns ratio $N = 1$.

Table 2.1: Design Example Construction Parameters

Parameter	Value
PCB Thickness	62 mil
PCB Layers	4
Copper Thickness	1 oz
Primary Turns	8
Secondary Turns	8
Clearance	14 mil
Air Gap	180 μm

The transformer is built using a three-dimensional finite element model and an exploded cross section is presented in Figure 2.1. The model includes the effect of the connections required to connect the transformer to an external circuit. This design example demonstrates the theory and procedure for extracting the transformer parasitic inductances, winding resistance, and capacitances at an operating frequency $f = 200kHz$.

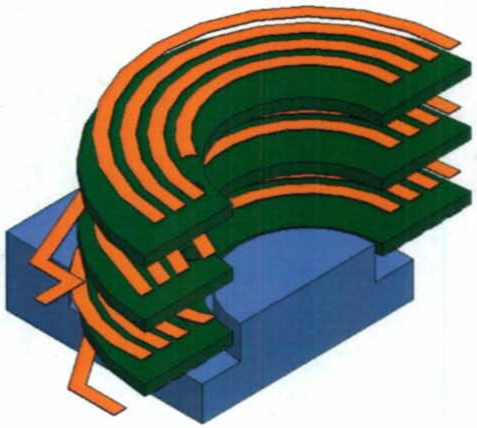

Figure 2.1: Design example: Planar transformer model.

2.3.1 Magnetizing Inductance

The magnetizing inductance (L_M) represents the strength of the magnetic coupling between the primary and the secondary of the transformer. L_M is measured at the primary of the transformer with the secondary open. The proposed methodology for measuring L_M in planar transformer simulations is:

1. Choose the eddy current solver with solution frequency $f = 200kHz$.
2. Apply a current excitation to the primary $I_p = 1A$.
3. Apply an open circuit current excitation to the secondary $I_s = 0A$.
4. Calculate the magnetic energy of the simulation using (2.20).

This operating condition is highlighted in Figure 2.2 and represents a transformer whose primary is generating a magnetic energy value equivalent to the magnetizing

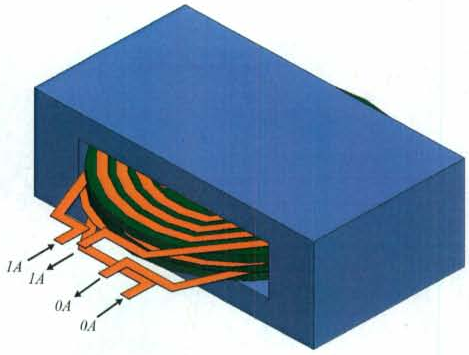

Figure 2.2: Operating condition to measure L_M.

inductance of the transformer with an open secondary. For this design example, the value of the magnetizing inductance obtained from the simulation was $L_M = 14.5\mu H$.

2.3.2 Leakage Inductance

The leakage inductance (L_{lk}) is a measure of the amount of magnetic flux which does not couple the primary to the secondary. L_{lk} is measured at the primary of the transformer with the secondary shorted. The proposed methodology of reproducing this procedure for finite element simulations is as follows:

1. Choose the eddy current solver with solution frequency $f = 200kHz$.
2. Apply a current excitation to the primary $I_p = 1A$.
3. Apply a short circuit current excitation to the secondary $I_s = 1A$.
4. Calculate the magnetic energy of the simulation using (2.20).

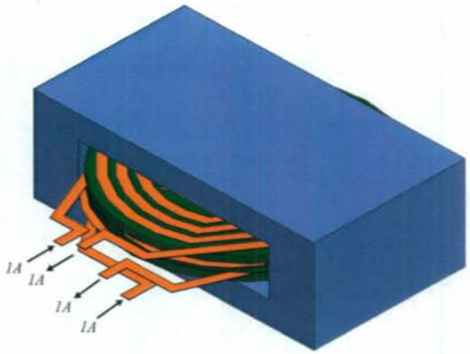

Figure 2.3: Operating condition to measure L_{lk}.

It is important that the secondary current provide equal and opposite amp-turns so that the measured energy accurately represents the leakage inductance of the transformer[34]. This operating condition is highlighted in Figure 2.3. For this design example the leakage inductance obtained from the simulation was $L_{lk} = 506nH$.

2.3.3 Winding Resistance

The winding resistance (R) represents the ohmic losses due to the copper traces without the effect of the magnetic core. To measure R, the core is removed and measurements are taken at the primary and secondary terminals to get a resistance value for each winding. For this example the windings are identical so only the primary resistance needs to be simulated. The procedure to simulate the resistance of the primary of the transformer for this example is as follows:

1. Remove the core and the secondary, leaving the primary and the primary dielectric.

2. Choose the eddy current solver with solution frequency $f = 200kHz$.

3. Apply a current excitation to the primary $I_p = 1A$.

4. Calculate the ohmic loss energy of the simulation using (2.22).

Figure 2.4: Operating condition to measure R.

This operating condition is highlighted in Figure 2.4. The resistance of the primary winding for this example was $R = 570m\Omega$

2.3.4 Inter-Winding Capacitance

The interwinding capacitance (C_{inter}) represents the capacitive energy stored between the primary and the secondary of the transformer. For this purpose the electrostatic solver will be used. To save time in the process the core is removed from the model since objects with high permeabilities and low permittivities have negligible effects on electrostatic simulations. The procedure to measure this capacitance in high frequency planar transformers is as follows:

1. Choose the electrostatic solver and remove the core from the model.

2. Apply a voltage excitation to the primary $V_p = 1V$.

3. Apply a voltage excitation to the secondary $V_s = 0V$.

4. Calculate the capacitive energy of the simulation using (2.7).

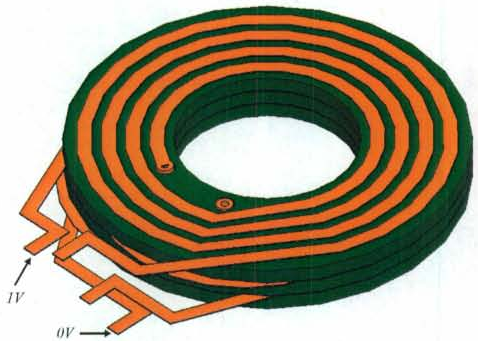

Figure 2.5: Operating condition to measure C_{inter}.

This operating condition is highlighted in Figure 2.5. The interwinding capacitance for this example was found to be $C_{inter} = 8.13pF$.

2.3.5 Intra-Winding Capacitance

The intra-winding capacitance (C_{intra}) represents the capacitive energy stored within the primary or the secondary winding. For this simulation both windings are identical, so simulating C_{intra} of the primary is sufficient to represent C_{intra} in the secondary. In this transformer the bulk of the capacitive energy is stored between the two layers of

Figure 2.6: Operating condition to measure C_{intra}.

the primary, so measuring the capacitance of the first layer with respect to the second layer of the primary is sufficient to represent C_{intra}. The procedure to simulate C_{intra} in a high frequency planar transformer is as follows:

1. Choose the electrostatic solver and remove the core and secondary from the model.
2. Remove the via which connects the two layers of the primary.
3. Apply a voltage excitation to the first layer of the primary $V_{p1} = 1V$.
4. Apply a voltage excitation to the second layer of the primary $V_{p2} = 0V$.
5. Calculate the capacitive energy of the simulation using (2.7).

This operating condition is highlighted in Figure 2.6. The intra-winding capacitance for this example was obtained as $C_{intra} = 14.2pF$.

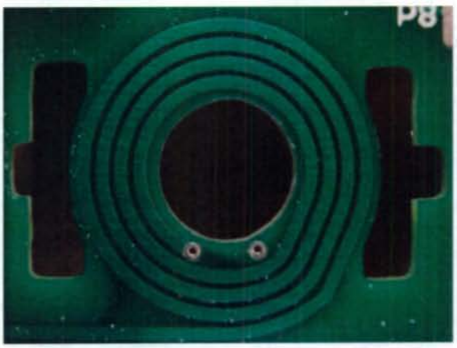

Figure 2.7: Experimental setup for measuring parasitics

2.3.6 Experimental Verification

A planar transformer with the same construction parameters was built and tested to confirm the validity of the described methods to calculate planar transformer parasitics. The experimental setup is presented in Figure 2.7 without the core to highlight the winding design. Parasitic values were measured with an LCR meter with an accuray of 0.1% and the comparative data is presented in Table 2.2.

Table 2.2: Design Example Results: Simulated vs. Experimental

Parasitic	Simulated	Experimental
L_M	14.5μH	14.8μH
L_{lk}	506nH	511nH
R	570mΩ	579mΩ
C_{inter}	8.13pF	8.23pF
C_{intra}	14.2pF	14.6pF

The resulting data is exceptionally accurate, with the predicted and experimental values matching within +/- 5%. The results from this design example highlight the effectiveness of using finite element simulations to simulate parasitic effects in high frequency planar transformers.

Chapter 3

Applying Response Surface Methodology to Planar Transformer Winding Design

3.1 Introduction

Finite element simulations provide an inexpensive and rapid way of verifying parasitic values for high frequency planar transformer designs as explained in Chapter 2. Unfortunately the process becomes iterative and time consuming if designing for the minimum resistance, or for a prescribed level of each parasitic. This chapter investigates and illustrates the use of Design of Experiment (DoE) methodology in conjunction with finite element simulation to develop mathematical models for each parasitic based on four winding design parameters highlighted in Figure 3.1: track width ratio ($\frac{a}{b}$), air gap length (l_g), clearance (d_c), and number of turns per winding

(N_w).

Twenty-five finite element simulations are performed on an isolation transformer built into a printed circuit board using an ER18/3/10 core set similar to the design example from Chapter 2. The resulting data is analyzed using DoE methodology and the result is a set of parametric models which are proven to be accurate and efficient tools for transformer design in Chapter 4.

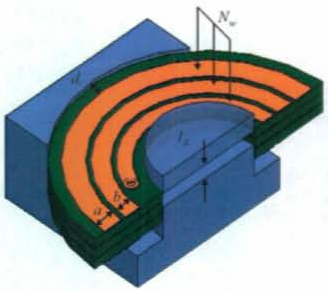

Figure 3.1: Planar transformer model highlighting winding design parameters

3.2 Design of Experiments Methodology

In this section, statistical Design of Experiments (DoE) methodology is explored to create accurate models for each parasitic element in planar transformers. Modeling the effects of every combination of transformer winding design factors (e.g., $\frac{a}{b}$, l_g, d_c, N_w, etc) using a mechanistic approach would require a significant time investment without gathering any information on interactions amongst the factors [35]. To take

an analytical approach to account for complicated factors such as the track width ratio requires approximation due to the highly nonlinear relationships between the parasitics and the factors. Statistical DoE methodology provides a systematic approach for applying statistics to experimentation to achieve efficient and accurate results [20].

3.2.1 Response Surface Methodology

Planar transformer parasitics are a complex, nonlinear, and multivariate system. To produce accurate parametric models for this complex system, Response Surface Methodology (RSM) is used [36]. The methodology employs regression analysis to provide parametric models of the form [20]

$$F(Y) = a_0 + \sum_{i=1}^{n} a_i x_i + \sum_{i=1}^{n} \sum_{j=1}^{n} b_{ij} x_i x_j \tag{3.1}$$

where Y is the response being measured, F represents a functional transform of Y (such as natural logarithm, or square root), a_0 is the overall average of measurements, a_i are linear regression coefficients, b_{ij} are quadratic and interaction regression coefficients, n represents the number of factors while x_i and x_j represent the factors being varied. These equations are valid over the factor ranges with an accuracy proportional to the adjusted R^2 value of the model.

Within RSM designs, the Central Composite Design (CCD) is very popular since it can be built upon a two-level factorial design [36]. CCD designs normalize all factor levels by coding the variables based on the scale: very low ($-\alpha$), low (-1), mid-point (0), high (+1) and very high ($+\alpha$). For this experiment the parameter for the very low and very high levels is $\alpha = 2$.

In order to minimize experimental runs while creating a robust quadratic parametric model, three measurement regions are considered:

1. Factorial experiments: Every combination of high and low levels of all factors (2^n measurements).
2. Mid-point experiment: All factors at their midpoint (1 measurement).
3. Axial experiments: One factor at very low or very high while the other factors are at their mid-point ($2n$ measurements).

In this chapter a four-factor CCD experiment used to model transformer parasitics based on winding design factors is described. With four factors the design requires 25 finite element simulations to completely characterize the parasitics over the range of the chosen factors. A four-layer PCB was simulated with a unity turns ratio to highlight the application of these results to isolation transformers.

3.2.2 Coded Factors

To interpret the results from the experiment it is important to understand the normalization procedure employed in the analysis. As mentioned, the factor levels are normalized within the range of -2 to +2 for this experiment. This abstracts the actual units and values of the factors from the actual analysis. A coded value of -2 represents the lowest factor value, 0 represents the midpoint, and +2 represents the highest level and all other values are linearly interpolated. Coded factors are denoted by a capital letter to highlight the normalization. For example, the normalized range of values of the track width ratio ($\frac{a}{b}$) is represented by the coded factor "A". All of the analysis in this chapter use coded factors.

Table 3.1: Factors Range of Operation

Factor	Coded	-2	-1	0	1	2	Units
Track Width Ratio ($\frac{a}{b}$)	A	0.98	0.99	1.00	1.01	1.02	
Air Gap Length (l_g)	B	60	120	180	240	300	μm
Clearance (d_c)	C	6	10	14	18	22	mil
Turns per Winding (N_w)	D	4	6	8	10	12	turns

3.3 Winding Design Parameters

The four factors investigated are the track width ratio ($\frac{a}{b}$), air gap length (l_g), clearance (d_c), and the number of turns per winding (N_w), which have been conceptually illustrated at the beginning of this chapter in Fig. 3.1. Table 3.1 presents the chosen factor levels and coded variables.

3.3.1 Track Width Ratio

The track width ratio (Factor A) represents the change in a turn's conductor width based on the proximity of the turn from the center of the core. To define the track widths, the winding breadth was divided into sixty blocks whose widths change by the track width ratio. These unevenly sized boxes are divided up evenly between the turns in each layer of the transformer, generating unevenly sized tracks as defined by the track width ratio. A track width ratio less than one signifies smaller conductor width near the center of the transformer as presented in Fig. 3.2. A track width ratio greater than one signifies thicker conductor near the center. The flux density plot contained in Fig. 3.3 indicates that the leakage flux density for a non-uniform

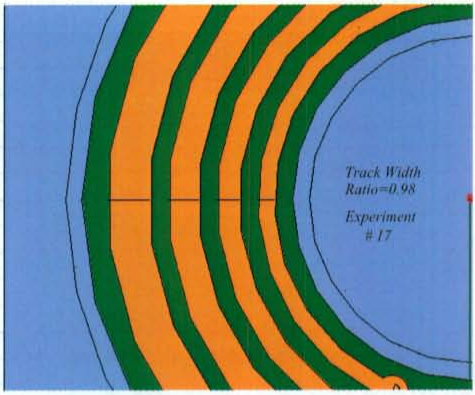

Figure 3.2: Top view of the 3D finite element model of a small planar transformer with a track width ratio less than one.

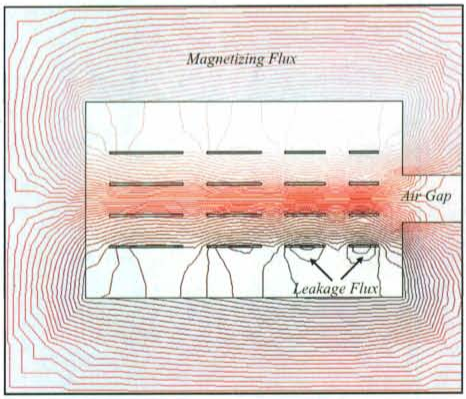

Figure 3.3: Magnetic flux line plot of a small planar transformer with a track ratio less than one.

track width is higher around the smaller conductor than the wider conductor. When the flux is concentrated near the center of the transformer, there is less volume for it to occupy, which indicates that a track width ratio less than one will provide less leakage inductance than a transformer with a track width ratio greater than one. A range from 0.98 to 1.02 was chosen for the ratio between blocks, which allows for the minimum manufacturable track width to be considered in the design.

3.3.2 Air Gap Length

The air gap length (Factor B) represents the spacing between the upper and lower core halves in the ER core set. The range from 60μm to 300μm was chosen to allow for all conventional air gap lengths to be represented within this range. Air gap length is traditionally used to manipulate L_M and will serve as a benchmark to establish the effect of the other factors on L_M.

3.3.3 Conductor Clearance

The clearance (Factor C) represents the distance between any two conductors, as well as the distance between any conductor and the core. The range from 6 mil to 22 mil represents the smallest manufacturable level to the level at which the conductor width reaches its minimum in conjunction with the track width ratio. By increasing the clearance, the copper width decreased so resistance is expected to increase.

3.3.4 Number of Turns

The number of turns per winding (Factor D) represents the number of turns in each of the primary and secondary windings. Since each winding has two identical layers, this factor represents the total number of turns across the two layers. The number of turns range from 4 to 12 per winding to accommodate the smallest manufacturable track width.

3.4 Parametric Models for Planar Transformer Parasitics

The responses are the transformer parasitics elements, namely magnetizing and leakage inductances (L_M, L_{lk}), inter and intra-winding capacitances (C_{inter}, C_{intra}), and winding resistance (R). These responses were measured using the inductive, resistive, and capacitive energy of the system in electromagnetic finite element simulations as discussed in Chapter 2. It is predicted that they will contain the same significant factors with different weightings. The resulting simulation results are contained in Table 3.2.

3.4.1 Parasitic Models

Applying RSM to the simulated parasitic data highlights the significant winding design factors ($\frac{a}{b}$,l_g,d_c,N_w) for each parasitic. The method applies a statistical significance test followed by quadratic regression analysis to produce the resulting parametric models as presented in (3.2) through (3.6). The parasitics are expressed in terms

Table 3.2: CCD Experimental Results

Run	A	B	C	D	$L_M(\mu H)$	$L_{lk}(nH)$	$R(m\Omega)$	$C_{inter}(pF)$	$C_{intra}(pF)$
1	-1	-1	-1	-1	12.8	264	114	9.06	17.1
2	+1	-1	-1	-1	12.3	282	132	9.11	16.3
3	-1	+1	-1	-1	7.60	264	114	9.06	17.1
4	+1	+1	-1	-1	7.40	282	132	9.11	16.3
5	-1	-1	+1	-1	12.5	292	342	8.08	13.5
6	+1	-1	+1	-1	12.6	309	351	7.89	13.4
7	-1	+1	+1	-1	7.50	292	336	8.08	13.5
8	+1	+1	+1	-1	7.50	309	360	7.89	13.4
9	-1	-1	-1	+1	35.0	734	807	8.97	15.6
10	+1	-1	-1	+1	35.0	775	909	8.71	15.5
11	-1	+1	-1	+1	20.8	734	796	8.97	15.6
12	+1	+1	-1	+1	20.7	775	876	8.71	15.5
13	-1	-1	+1	+1	34.8	844	1748	6.94	10.9
14	+1	-1	+1	+1	34.7	866	1900	6.91	10.7
15	-1	+1	+1	+1	20.9	844	1723	6.94	10.9
16	+1	+1	+1	+1	20.6	866	1782	6.91	10.7
17	-2	0	0	0	15	488	575	7.55	13.4
18	+2	0	0	0	16	551	718	8.07	14.0
19	0	-2	0	0	38.5	507	584	8.13	14.2
20	0	+2	0	0	10.5	503	566	8.13	14.2
21	0	0	-2	0	16	459	402	9.65	17.8
22	0	0	+2	0	13.2	577	1110	6.39	10.0
23	0	0	0	-2	4.5	126	125	8.94	16.3
24	0	0	0	+2	36	1160	2050	7.82	12.7
25	0	0	0	0	14.5	506	570	8.13	14.2

of each physical coded variable (A, B, C, and D) under investigation. The equations represent a clear nonlinear trend with high complexity as shown by the number of interactions (products between two variables) and higher order terms.

$$L_M = 15.09 - 5.53B + 8.55D - 2.27BD + 2.40B^2 + 1.34D^2 \tag{3.2}$$

$$\begin{aligned} L_{lk} = {} & 516.59 + 13.33A - 0.36B + 31.21C + 258.85D \\ & - 2.59AC + 3.28AD + 18.26CD - 2.80B^2 + 31.79D^2 \end{aligned} \tag{3.3}$$

$$\begin{aligned} R = {} & 268.89 + 17.71A + 88.4C + 202.97D + 78.12CD + 9.66A^2 \\ & + 18.32C^2 + 47.28D^2 \end{aligned} \tag{3.4}$$

$$C_{inter} = 8.15 + 0.08A - 0.77C - 0.31D - 0.20CD - 0.065A^2 + 0.078D^2 \tag{3.5}$$

$$C_{intra} = 14.08 - 0.05A - 1.98C - 0.93D - 0.39CD - 0.09A^2 + 0.12D^2 \tag{3.6}$$

These models are determined to be statistically significant with exceptional fit. The adjusted R^2 values, which indicate the quality of fit between the model and the data contained in Table 3.2, for each model are 0.9863, 0.9998, 0.9877, 0.9797, and 0.9919 respectively. This shows an exceptional correlation considering the theoretical maximum R^2 value is 1.0. The detailed ANOVA data for each model are contained in Appendix A. These five responses are considered to be essentially independent since there is no exact relationship between them. However, it should be noted that the predicted models for C_{inter} and C_{intra} contain the same factors, thus following a similar trend.

The trends indicated by these models are intuitive and insightful. For example, the positive effect of the clearance (Factor C) and the number of turns (Factor D) on the resistance is expected since the conductor length and width are decreased, increasing the current density and thus the loss. The interaction term CD in the

response shows that there is an interaction between the effect of clearance and the number of turns, a term which is missed in one-factor experiments. The interaction plots associated with all models have been included in Appendix B. It is also expected that the air gap length (Factor B) does not affect the winding resistance as explained in Chapter 2. Great insight is gained into the effect of the track width ratio (Factor A) on the winding resistance. The quadratic nature of the A^2 term in the Resistance allows for the possibility of a track width ratio which gives a minimum resistance, which allows for the possibility of an optimal design.

3.4.2 Response Surfaces

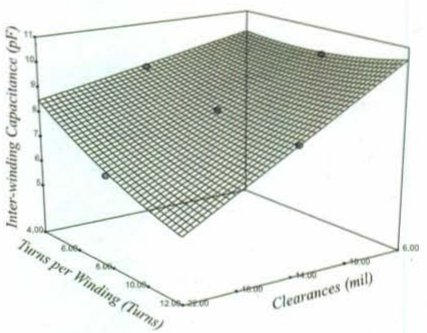

Figure 3.4: Response surface of C_{inter}

RSM allows for rapid prototyping and design of parasitic values, through the use of the response surfaces. The response surfaces of the transformer parasitics capture their nonlinearity, highlight factor interactions, and give all of the possible operating points within the factor ranges. The interaction between the clearance and

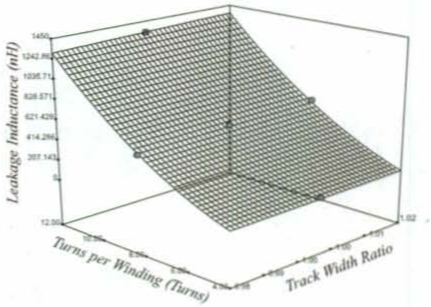

Figure 3.5: Response surface of L_{lk}

the number of turns can be seen from the irregular shape in the response surface of the inter-winding capacitance in Figure 3.4 while the nonlinearity of the leakage inductance with respect to the number of turns is shown in its response surface in Figure 3.5.

3.4.3 Track Width Ratio Significance

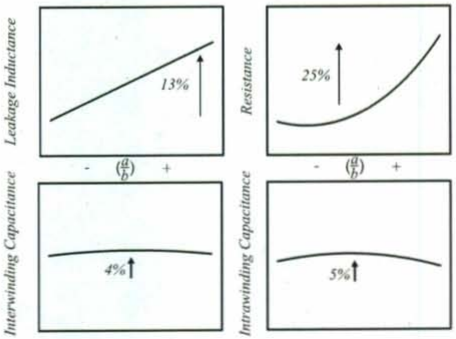

Figure 3.6: Parasitic trends with increasing track width ratio.

As a result of this work, an important effect associated with the track width ratio has been identified. The simulations revealed that increasing track width ratio by 4% increased the leakage inductance by 13% and resistance by 25%, but only increases the inter-winding capacitance by 4% and the intra-winding capacitance by 5%, as represented in Fig. 3.6. These trends are in line with the predictions based on the magnetic flux plot presented in Fig. 3.3, in that the leakage flux concentrates around the thinner conductors, so minimizing the volume of the smaller conductors will minimize leakage inductance. The resistance trend is insightful as it indicates that there is a minimum resistance point with a track width ratio less than one. Under this condition the overall resistance is decreased due to a more even distribution of resistance per turn, which is counteracted at low track width ratios by the resistance of the very thin inner turn. This becomes an optimization problem to find the track width ratio which supplies the lowest resistance. Determining the minimum resistance point creates excellent gains in efficiency considering the resistance can change by up to 25%. While the track width ratio changes the distribution of the copper in the winding window, it does not change the total width of copper used, which means the total cross sectional area of copper is constant. This means the capacitance will not be significantly affected by the track width ratio. This is an important observation as it allows the leakage inductance of a planar transformer to be tuned independently from the capacitances.

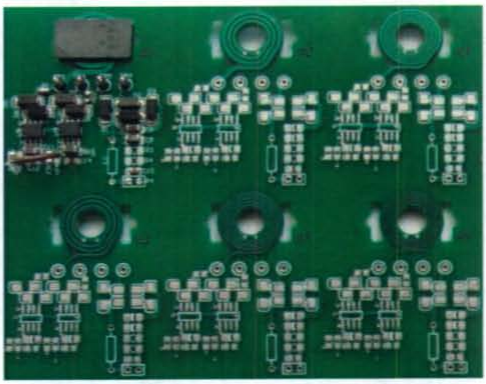

Figure 3.7: Experimental validation test board. Setup # 1 is the design example transformer and setups 2 - 6 are the five test points.

3.4.4 Experimental Validation

To highlight the exceptional accuracy of the proposed method five experimental validation runs were performed using the printed circuit board presented in Fig. 3.7. The board shows six transformers with auxiliary power electronics. The one that is populated is the one which was used in the ensuing LLC converter design example in Chapter 4 while the remaining five of these were tested to compare the results of all responses with those shown in (3.2) through (3.6). The excellent match for the resistance and inter-winding capacitance are highlighted in Fig. 3.8 and Fig. 3.9 respectively. These results indicate that rapid prototyping using a combination of Design of Experiment methodology and finite element analysis allows for accurate and inexpensive models over a wide range of winding design parameter values.

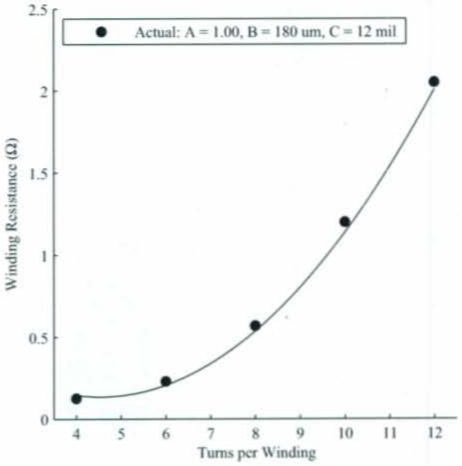

Figure 3.8: Resistance: actual (circles) vs. predicted (smooth line).

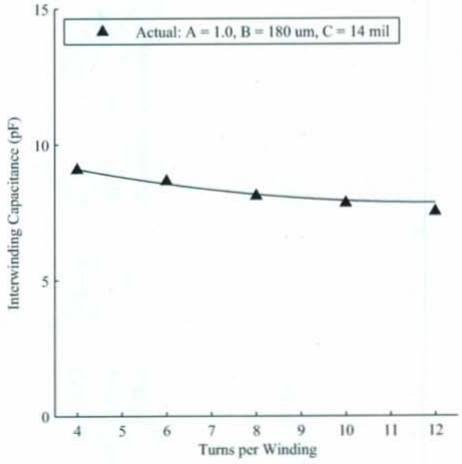

Figure 3.9: Inter-winding capacitance: actual (triangles) vs. predicted (smooth line).

Chapter 4

Integrated Magnetic Design of Planar Transformers for LLC Resonant Converters

4.1 Introduction

The proposed methodology for the prediction of planar transformer parasitics in Chapter 3 allows for rapid design of transformers with prescribed parasitic levels. In this chapter a set of design guidelines for planar transformers for a 2.5W LLC resonant converter using the previously obtained parametric models is proposed. A planar transformer prototype was designed and tested within a 2.5W LLC resonant converter and results under different operating modes are included to illustrate the resonant behavior and to validate the presented design procedure.

4.2 LLC Converter Operation

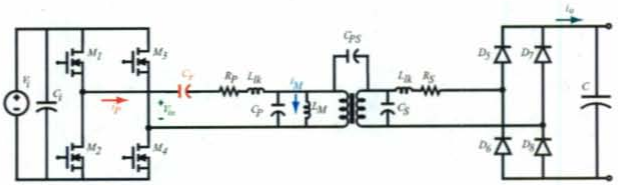

Figure 4.1: Full-bridge LLC resonant converter with transformer parasitics.

LLC resonant converters provide the benefit of soft transitions to reduce switching losses and can operate at very high frequencies. In particular, LLC resonant converters have gained popularity due to their Zero Voltage Switching (ZVS) turn-on and Zero Current Switching (ZCS) turn-off operation under a wide range of loading conditions, including no load condition [37, 38, 39]. LLC converters use passive magnetic resonance between a series inductor (L_r), series capacitor (C_r) and a parallel inductance (L_p) placed between the switches and the rectifier of a DC-DC converter. In this chapter the series and parallel inductances will be replaced by the transformer L_{lk} and L_M as highlighted in Figure 4.1. These magnetic parameters affect the converter's operation through modifying the operating frequency range, the switching operation (ZVS or ZCS), and the load regulation capability. A family of curves highlighting the LLC DC characteristics are presented in Fig. 4.2 with changing load condition. Frequency f_{r2} presented in Fig. 4.2 is the resonant frequency at which the series capacitance resonates with the combined series and magnetizing inductances and f_{r1} is the frequency at which the series capacitor resonates with only the leakage induc-

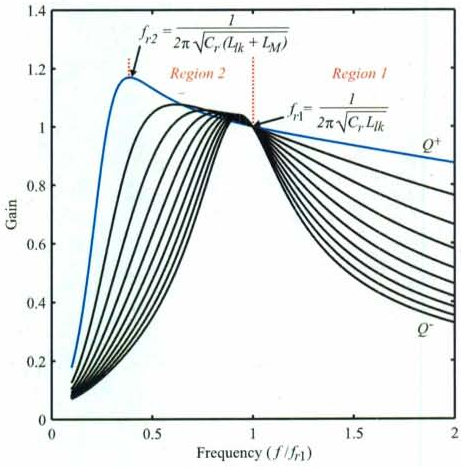

Figure 4.2: Conceptual LLC resonant converter gain vs. frequency characteristic with changing load condition, Q.

tance. The converter operates under ZCS condition when the slope of the gain vs. frequency curve is positive and operates under ZVS when the slope is negative. The switching losses in the MOSFETs are reduced under ZVS condition so the converter must be operated in either Region 1 or Region 2, as indicated in Fig. 4.2 with dashed lines. The load regulation is determined by the slope of the curve, which is greatly affected by the magnetizing inductance. The lower the magnetizing inductance, the higher the slope of the curve which means more effective regulation capabilities over a small frequency range.

As can be seen, the operation of the LLC resonant converter is highly dependent on the interaction between C_r, L_{lk} and L_M. As will be seen, the high accuracy prediction models using Response Surface Methodology proposed in Chapter 3 can reduce the number of components required in resonant DC-DC converters by controlling L_{lk} and L_M to fulfill the requirements of resonant converters. For this purpose, the following sections outline an LLC case study and non-iterative design procedure to highlight the effectiveness of the parasitic models in LLC planar transformer design.

4.3 Transformer Design Specifications

The LLC converter proposed for this design has specifications described in Table 4.1. The resultant transformer parasitic requirements are presented in Table 4.2, from the relations presented in Figure 4.2 using a series capacitance $C_r = 1\mu F$.

Table 4.1: LLC Converter Design Parameters

Parameter	Value
First Resonant Frequency (f_{r1})	200 kHz
Second Resonant Frequency (f_{r2})	30 kHz
V_{in}	10 V
Turns Ratio	1:1
R_{load}	40 Ω

Table 4.2: Transformer Design Parameters

Parasitic	Design Value
Magnetizing Inductance	26 μH
Leakage Inductance	600 nH
Resistance	Minimum
Capacitances	Minimum

4.4 Design Procedure

Using the parasitic prediction models presented in (3.2) through (3.6) a design procedure for a planar transformer for a 2.5W LLC resonant converter is developed. To meet the parasitic requirements the following design procedure is recommended:

1. Define the minimum number of turns (Factor D in coded units), based on rated voltage and frequency:

   The minimum number of turns for this application is determined by the saturation of the core, from the relation[40]

   $$N_{wmin} = \frac{V_o \times 10^4}{4Ae_{min}\Delta Bf} \tag{4.1}$$

   which, for an ER 18/3.2/10 core set with a maximum flux density of 200mT, results in a minimum of eight turns (D = 0) being employed.

2. Use (3.2) with D = 0 to find the air gap (Factor B) which obtains the desired magnetizing inductance of 26 μ H:

   $$B = -1.27 \tag{4.2}$$

   This suggests the coded value of the required airgap is -1.27 which lies between l_g = 60 μm (B = -2) and l_g = 120 μm (B = -1). The exact air gap required to produce a magnetizing inductance of 26 μH is 100 μm.

3. Use the response surface of (3.3) to find all of the combinations of clearance (Factor C) and track width ratio (Factor A), which obtain the desired leakage inductance.

4. Use (3.4),(3.5), and (3.6) simultaneously to choose the combination of clearance and track width ratio which minimizes resistance and capacitance while still producing the desired leakage inductance. Solving these equations simultaneously provides one possible solution of 16 mil clearance and 0.995 track width ratio. This allows for a leakage inductance value of 600 nH while minimizing the resistance ($505m\Omega$) and inter and intra-winding capacitances ($12.3pF$ and $7.1pF$).

This design procedure is quick and flexible, allowing precision control of parasitics without iteration. The resulting winding design parameters for the transformer are summarized in Table 4.3.

Table 4.3: Planar Transformer Winding Design Parameters

Parameter	Rating
Track Width Ratio	0.995
Air Gap Length	100 μm
Clearance	16 mil
Turns per Winding	8

4.5 Experimental Prototype

The designed transformer was constructed using a four layer printed circuit board and an ER18/3/10 core set with 1 oz copper traces. The resulting LLC converter, including auxiliary power electronics is presented in Figure 4.3. The converter was

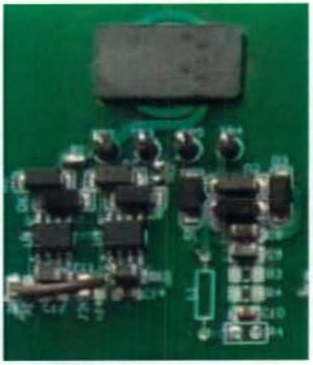

Figure 4.3: LLC converter including design example transformer

tested to observe the appropriate gain vs. frequency response and the waveforms were tested in Region 1 and Region 2 to confirm the resonant behavior.

4.5.1 Experimental Results

Table 4.4: Transformer Parasitic Levels

Parasitic	Designed	Finite Element	Experimental	% Error
L_M (μH)	26	25.8	26.5	1.9
L_{lk} (nH)	600	588	619	3.2
R (mΩ)	505	494	528	4.6
C_{inter} (pF)	12.3	12.0	12.7	3.3
C_{intra} (pF)	7.1	6.9	7.2	1.4

The proposed transformer was designed using the specifications outlined above

with the parasitic levels indicated in Table 4.2. The construction provided very accurate results in terms of the predicted parasitics as presented in Table 4.4. Only a small amount of the total parasitic levels were contained in the final construction that were not accounted for in the parametric models. The final transformer contains parasitic levels which contain less than 5% error compared to the desired values, highlighting the excellent accuracy of DoE methodology combined with finite element analysis.

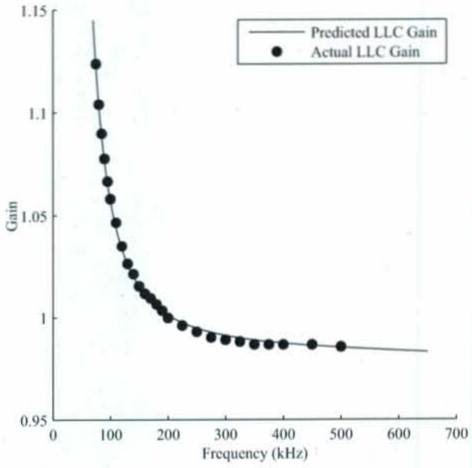

Figure 4.4: LLC converter gain vs. frequency characteristic: actual vs. predicted.

The gain vs. frequency plot shows excellent correlation between theoretical and experimental behavior and is presented in Figure 4.4. The load regulation is excellent within the region investigated, ranging from a gain of 0.98 to 1.12 over the frequency range of 100 kHz to 500 kHz.

To conclude the testing, the converter was operated over Regions 1 and 2 and the waveforms were analyzed compared to simulated waveforms. Figures 4.5 and 4.6 highlight the simulated and experimental waveforms from Region 1 while Figures 4.7 and 4.8 highlight the simulated and experimental waveforms for Region 2. In Region 1, it behaves as a series resonant converter, so the magnetizing inductance does not resonate with the series capacitance because it is clamped to the output voltage. In Region 2 there is a combination of series and parallel converter behavior. The output current becomes discontinuous, which isolates the output from the transformer for a portion of the cycle, allowing the magnetizing inductance to resonate with the series inductance and capacitance. Both of these behaviors are observed in the experimental results, confirming the accuracy of this design procedure.

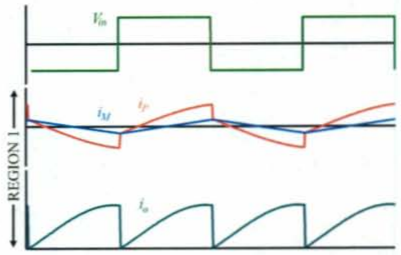

Figure 4.5: LLC simulation waveforms operating in Region 1: voltage applied to resonant tank, primary current, and secondary current.

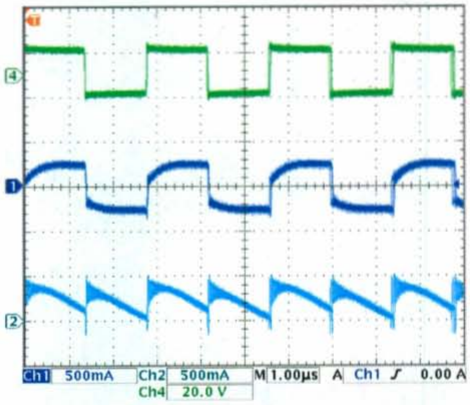

Figure 4.6: LLC case study waveforms operating in Region 1: voltage applied to resonant tank (Ch4), primary current (Ch1), and secondary current (Ch2).

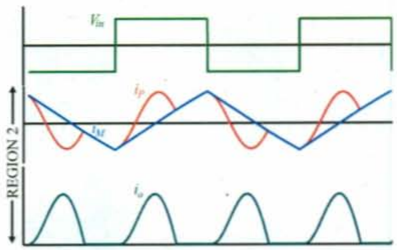

Figure 4.7: LLC simulation waveforms operating in Region 2: voltage applied to resonant tank, primary current, and secondary current.

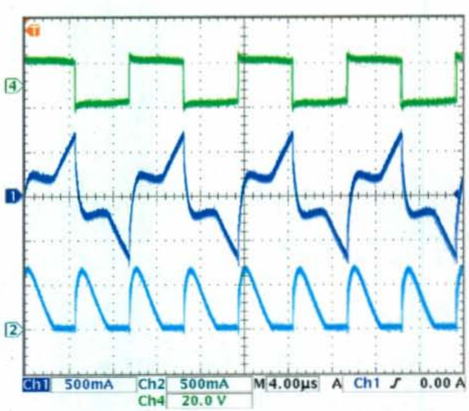

Figure 4.8: LLC case study waveforms operating in Region 2: voltage applied to resonant tank (Ch4), primary current (Ch1), and secondary current (Ch2).

Chapter 5

Conclusions

The winding design of planar transformers is a challenging trade off process in which the winding structure affects the transformer's electromagnetic, thermal, power flow, and parasitic behavior simultaneously. Focusing on the parasitic elements, these arrangements cause the transformer to display different levels of magnetizing and leakage (L_M and L_{lk}), inter and intra-winding capacitances (C_{inter} and C_{intra}), and winding resistance (R). This work provided the methodology required to generate high accuracy prediction models for transformer parasitics based on various winding design parameters, specifically: track width ratio, air gap length, conductor clearance, and number of turns per winding. The models were generated using a combination of finite element modeling (FEM) and Design of Experiment (DoE) methodology. Planar transformers, using an ER18/3/10 core set, built into printed circuit boards were employed to characterize planar transformer parasitics over a wide range of winding design parameters.

Chapter 2 provided analysis and simulation procedures for extracting parasitics

from high frequency planar transformer models. FEM is shown to be an accurate and efficient method of electromagnetically modeling high frequency planar transformers using a combination of electrostatic, magnetostatic, and eddy current solvers. Methods to reduce simulation time by selectively choosing which model objects to include in each simulation were discussed, as well as the proper excitations required for parasitic extraction. A design example was provided to highlight the accuracy of the proposed methods.

Chapter 3 extended the parasitic prediction models to a wide range of winding design parameters using a Central Composite Design (CCD) experiment based on twenty-five finite element simulations. The results from the CCD experiment were a set of quadratic parametric equations based on the investigated factors. The resulting equations highlighted the high nonlinearity of planar transformer parasitics as well as the complexity due to interactions amongst winding design parameters. The most interesting and insightful discovery from the experiment was the effect of the track width ratio. The experiment revealed that the track width ratio caused a minimum in R while having a significant impact on L_{lk} and no significant effect on C_{inter} or C_{intra}. The high accuracy of this approach and the resulting discoveries were confirmed using five experimental test transformers.

Chapter 4 presented a non-iterative method for designing planar transformers for use in LLC resonant converters based on parasitic prediction models developed in Chapter 3. The method was shown to be quick and efficient once the parametric model is extracted, requiring four simple steps. Experimetal parasitic levels excellently matched predicted values, and a 2.5W LLC converter prototype using an ER18/3.2/10 core set in a four layer printed circuit board has been successfully tested to confirm

the validity of the approach.

The contributions of the work are demonstrated by the following publications on the use of CCD experiments in planar transformer design:

- Samuel R. Cove, Martin Ordonez, and John E. Quaicoe, "Modeling of Planar Transformer Parasitics Using Design of Experiment Methodology," *IEEE Canadian Conference on Electrical and Computer Engineering*, CCECE 2010, Calgary (Canada), May 2010.

- Samuel R. Cove, Martin Ordonez, Federico Luchino, and John E. Quaicoe, "Applying Response Surface Methodology to Planar Transformer Winding Design," *IEEE Energy Conversion Congress and Expo*, ECCE 2010, Atlanta (USA), Sept. 2010.

- Samuel R. Cove, Martin Ordonez, Federico Luchino, and John E. Quaicoe, "Integrated Magnetic Design of Small Planar Transformers for LLC Resonant Converters" *IEEE Energy Conversion Congress and Expo*, ECCE 2011, Submitted for review.

- Samuel R. Cove, Martin Ordonez, Federico Luchino, and John E. Quaicoe, "Applying Response Surface Methodology to Small Planar Transformer Winding Design" *IEEE Transactions on Industrial Electronics*, Submitting Winter 2011.

5.1 Future Work

The work presented in this thesis is only the beginning of an in-depth study of the design of planar transformers for use in parasitic-sensitive converters. The methodology to generate the parasitic prediction models is applicable to any size of core and core geometry, but the design procedure needs to be verified as applicable for various core sizes and shape.

The track width ratio concept is novel and requires further investigation to confirm its behavior over a wide range of ratios. The current models for leakage inductance are linear but there is a belief that if a wider range were investigated there would be a global minimum. The challenge will be to find this point for various numbers of turns and core shapes and to compare it to the minimum resistance point.

In this current work, the LLC transformer design example only integrated the leakage inductance and the magnetizing inductance into the design. There are integrated planar magnetic structures which can incorporate the series capacitance as well. However, these structures are more complicated to design. The goal is to create a design procedure for a fully integrated structure which can predict all three of these parameters as well as resistance and the stray capacitances to optimize the design of integrated magnetic structures.

Bibliography

[1] Farid Amalou, Etienne L. Bornand, and Martin A. M. Gijs. Batch-type millimeter-size transformers for miniaturized power applications. *IEEE Transactions on Magnetics*, 37(4):2999–3003, 2001.

[2] Wei Chen, Yipeng Yan, Yuequan Hu, and Qing Lu. Model and design of pcb parallel winding for planar transformer. *IEEE Transactions on Magnetics*, 39(5):3202–3204, 2003.

[3] Erik C. W. de Jong, Braham J. A. Ferreira, and Pavol Bauer. Toward the next level of pcb usage in power electronic converters. *IEEE Transactions on Power Electronics*, 23(6):3151–3163, 2008.

[4] Ali I. Maswood and Lim Keng Song. Design aspects of planar and conventional smps transformer: A cost benefit analysis. *IEEE Transactions on Power Electronics*, 50(3):571–577, 2003.

[5] N. Dai, A. W. Lotfi, G. Skutt, W. Tabisz, and F. C. Lee. A comparative study of high frequency low profile planar transformer technologies. In *Proceedings of the Applied Power Electronics Conference*, pages 226–232, Feb. 1994.

[6] P. M. Gradski and Fred C. Lee. Design of high-frequency hybrid power transformer. In *Proceedings of the Applied Power Electronics Conference*, pages 319–326, Feb. 1988.

[7] W. J. B. Heffernan, P. D. Evans, and W. M. Chew. A comparison of high frequency power transformer topologies. In *Proceedings of the European Conference on Power Electronics and Applications*, pages 25–30, Sept. 1991.

[8] S. Ramakrishnan, R. Steigerwald, and J. A. Mallick. A comparison study of low-profile power magnetics for high frequency high density switching converters. In *Proceedings of the Applied Power Electronics Conference*, pages 388–394, Feb. 1997.

[9] J. A. Sabaté, V. Vlatkovic, R.B. Ridley, F.C. Lee, and B. H. Cho. Design considerations for high-voltage high-power full-bridge zero-voltage-switched pwm converter. In *Proceedings of the Applied Power Electronics Conference*, Mar. 1990.

[10] Kwang-Hwa Liu and Fred C. Y. Lee. Zero-voltage switching technique in dc/dc converters. *IEEE Transactions on Power Electronics*, 5(3):293, 1990.

[11] Chuan-Sheng Liu, Liang-Rui Chen, B. Z. Li, and Z. P. Huang. The implementation of a full-bridge phase-shifted zero-voltage-switching power converter. In *Proceedings of the International Conference on Power Electronics and Drive Systems*, Nov. 2009.

[12] Young-Do Kim, Chong-Eun Kim, Kyu-Min Cho, Ki-Bum Park, and Gun-Woo Moon. Zvs phase shift full bridge converter with controlled leakage inductance

of transformer. In *Proceedings of the International Telecommunications Energy Conference*, Oct. 2009.

[13] Bo Yang. *Topology Investigation for Front End DC/DC Power Conversion for Distributed Power System*. PhD thesis, Virginia Polytechnic Institute and State University, 2003.

[14] R. L. Steigerwald. A comparison of half-bridge resonant converter topologies. *IEEE Transactions on Power Electronics*, 3(2):174, 1988.

[15] Ray-Lee Lin and Chiao-Wen Lin. Design criteria for resonant tank of llc dc-dc resonant converter. In *Proceedings of the Conference on IEEE Industrial Electronics Society*, Nov. 2010.

[16] Byoung-Hee Lee, Moon-Young Kim, Chong-Eun Kim, Ki-Bum Park, and Gun-Woo Moon;. Analysis of llc resonant converter considering effects of parasitic components. In *Proceedings of the Telecommunications Energy Conference*, Oct. 2009.

[17] Ray-Lee Lin and Chiao-Wen Lin. Efficiency study for a 150w llc resonant converter. In *Proceedings of the International Conference on Power Electronics and Drive Systems*, Nov. 2009.

[18] Jee hoon Jung and Joong gi Kwon. Theoretical analysis and optimal design of llc resonant converter. In *Proceedings of the European Conference on Power Electronics and Applications*, Sep. 2007.

[19] Ching-Ming Lai, Rong-Chyang Lee, Te-Wei Wang, and Kuo-Kai Shyu. Design and implementation of a single-stage llc resonant converter with high power factor. In *Proceedings of the IEEE International Symposium on Industrial Electronics*, Jun. 2007.

[20] D. C. Montgomery. *Design and Analysis of Experiments*. John Wiley and Sons, fifth edition, 2001.

[21] Jianbing Li, Changchao Hu, and Xuemin Pang. Analysis of the leakage inductance of planar transformer. In *Proceedings of the International Conference on Electronic Measurement & Instruments*, Aug. 2009.

[22] Ziwei Ouyang, Ole C. Thomsen, and Michael A. E. Andersen. The analysis and comparison of leakage inductance in different winding arrangements for planar transformer. In *Proceedings of the International Conference on Power Electronics and Drive Systems*, Nov. 2009.

[23] Heng-Ming Hsu and Chien-Wen Tseng. Design of on-chip transformer with various coil widths to achieve minimal metal resistance. *IEEE Electron Device Letters*, 28(11):1029–1032, 2007.

[24] Frédéric Robert, Pierre Mathys, , and Jean-Pierre Schauwers. A closed-form formula for 2-d ohmic losses calculation in smps transformer foils. *IEEE Transactions on Power Electronics*, 16(3):437–444, 2001.

[25] Mika Sippola and Raimo E. Sepponen. Accurate prediction of high-frequency power-transformer losses and temperature rise. *IEEE Transactions on Power Electronics*, 17(5):835–847, 2002.

[26] Luca Dalessandro and and Johann W. Kolar Fabiana da Silveira Cavalcante. Self-capacitance of high-voltage transformers. *IEEE Transactions on Power Electronics*, 22(5):1105–1112, 2007.

[27] Hai Yan Lu, Jian Guo Zhu, and S. Y. Ron Hui. Experimental determination of stray capacitances in high frequency transformers. *IEEE Transactions on Power Electronics*, 18(5):1105–1112, 2003.

[28] Djordje Garabandic, William G. Dunford, and Mark Edmunds. Zero-voltage zero-current switching in high-output-voltage full-bridge pwm converters using the interwinding capacitance. *IEEE Transactions on Power Electronics*, 14(2):343–349, 1999.

[29] Ruowen Rong, D. A. Lowther, Z. Malik, Hua Su, J. Nelder, and R. Spence. Applying response surface methodology in the design and optimization of electromagnetic devices. *IEEE Transactions on Magnetics*, 33(2):1916–1919, 1997.

[30] Do-Kwan Hong, Ki-Chang Lee, Byung-Chul Woo, and Dae-Hyun Koo. Optimum design of electromagnet in magnetic levitation system for contactless delivery application using response surface methodology. In *Proceedings of the International Conference on Electric Machines*, Sept. 2008.

[31] H.G. Cheon, D.S. Kwag, J.H. Choi, C.H. Min, T.S. Park, H.H. Kim, and S.H. Kim. Insulation design and experimental results for transmission class hts transformer with composite winding. *IEEE Transactions on Superconductivity*, 18(2):648–651, 2008.

[32] Samuel R. Cove, Martin Ordonez, and John E. Quaicoe. Modeling of planar transformer parasitics using design of experiment methodology. In *Proceedings of the IEEE Canadian Conference on Electrical and Computer Engineering*, May 2010.

[33] Peter P. Silvester and Ronald L. Ferrari. *Finite Elements for Electrical Engineers*. Cambridge University Press, third edition, 1996.

[34] Ansoft Corporation. Principles of emss. *Ansoft EMSS Engineering Note*, page 17, 2003.

[35] Veronica Czitrom. One-factor-at-a-time versus designed experiments. *The American Statistician*, 53(2):126–131, 1999.

[36] R. Myers and D.C. Montgomery. *Response Surface Methodology: Process and Product Optimization Using Designed Experiments*. John Wiley and Sons, second edition, 2003.

[37] Reza Beiranvand, Bizhan Rashidian, Mohammad Reza Zolghadri, and Seyed Mohammad Hossein Alavi. Using llc resonant converter for designing wide-range voltage source. *IEEE Transactions on Industrial Electronics*, Available in IEEE Xplore forthcoming articles, 2011.

[38] Saichol Chudjuarjeen, Anawach Sangswang, and Chayant Koompai. An improved llc resonant inverter for induction heating applications with asymmetrical control. *IEEE Transactions on Industrial Electronics*, Available in IEEE Xplore forthcoming articles, 2011.

[39] Jun-Young Lee, Yu-Seok Jeong, and Byung-Moon Han. An isolated dc/dc converter using high-frequency unregulated llc resonant converter for fuel cell applications. *IEEE Transactions on Industrial Electronics*, Available in IEEE Xplore forthcoming articles, 2011.

[40] Ned Mohan, Tore M. Undeland, and William P. Robbins. *Power Electronics: Converters, Applications, and Design.* John Wiley and Sons, first edition, 2006.

Appendix A

Parametric Models: ANOVA Data

Analysis of variance (ANOVA) is a critical part of assessing the quality of the fit of proposed parametric models [20]. ANOVA is used to determine which factors are significant, how each factor should be weighted, and the accuracy of the resulting model. The following ANOVA tables confirm the choice of parametric models by confirming each factor's significance through its associated p-value. For this analysis, a p-value less than 0.1 indicates a significant factor, and should be included in the resulting model. The exception to this rule is when a second order term is considered significant (A^2, B^2, AB, etc.) but the associated first order term (A,B,C, etc.) is insignificant. A model should remain hierarchical so if the factor AB is considered significant then factors A and B must be included in the model regardless of their significance [20]. The ANOVA data also indicates the adjusted R^2 value for each model with indicates the quality of the fit of the model. An adjusted R^2 value close to 1.0 indicates a highly accurate fit to the simulation data which was used to develop the model.

ANOVA for Response Surface Reduced Quadratic Model

Analysis of variance table [Partial sum of squares - Type III]

Source	Sum of Squares	df	Mean Square	F Value	p-value Prob > F	
Model	2715.38	5	543.08	274.24	< 0.0001	significant
B-Air Gap	*733.72*	*1*	*733.72*	*370.52*	*< 0.0001*	
D-Turns	*1756.17*	*1*	*1756.17*	*886.84*	*< 0.0001*	
BD	*82.36*	*1*	*82.36*	*41.59*	*< 0.0001*	
B^2	*132.26*	*1*	*132.26*	*66.79*	*< 0.0001*	
D^2	*41.06*	*1*	*41.06*	*20.73*	*0.0002*	
Residual	37.62	19	1.98			
Cor Total	2753.01	24				

Std. Dev.	1.41	R-Squared	0.9863
Mean	18.68	Adj R-Squared	0.9827
C.V. %	7.53	Pred R-Square	0.9483
PRESS	142.40	Adeq Precisior	49.633

Figure A.1: ANOVA statistics for L_M parametric model.

ANOVA for Response Surface Reduced Quadratic Model

Analysis of variance table [Partial sum of squares - Type III]

Source	Sum of Squares	df	Mean Square	F Value	p-value Prob > F	
Model	1.668E+006	9	1.853E+005	8657.51	< 0.0001	significant
A-TWR	*4320.17*	*1*	*4320.17*	*201.85*	*< 0.0001*	
B-Air Gap	*2.67*	*1*	*2.67*	*0.12*	*0.7290*	
C-Clearance	*23312.67*	*1*	*23312.67*	*1089.22*	*< 0.0001*	
D-Turns	*1.608E+006*	*1*	*1.608E+006*	*75123.09*	*< 0.0001*	
AC	*100.00*	*1*	*100.00*	*4.67*	*0.0472*	
AD	*196.00*	*1*	*196.00*	*9.16*	*0.0085*	
CD	*5329.00*	*1*	*5329.00*	*248.98*	*< 0.0001*	
B^2	*177.14*	*1*	*177.14*	*8.28*	*0.0115*	
D^2	*23120.53*	*1*	*23120.53*	*1080.24*	*< 0.0001*	
Residual	321.05	15	21.40			
Cor Total	1.668E+006	24				

Std. Dev.	4.63	R-Squared	0.9998
Mean	544.36	Adj R-Squared	0.9997
C.V. %	0.85	Pred R-Square	0.9996
PRESS	683.22	Adeq Precisior	353.843

Figure A.2: ANOVA statistics for L_{lk} parametric model.

ANOVA for Response Surface Reduced Quadratic Model

Analysis of variance table [Partial sum of squares - Type III]

Source	Sum of Squares	df	Mean Square	F Value	p-value Prob > F	
Model	8.938E+006	6	1.490E+006	240.32	< 0.0001	significant
A-TWR	*23312.67*	*1*	*23312.67*	*3.76*	*0.0683*	
C-Clearance	*1.539E+006*	*1*	*1.539E+006*	*248.31*	*< 0.0001*	
D-Turns	*6.521E+006*	*1*	*6.521E+006*	*1051.93*	*< 0.0001*	
CD	*5.141E+005*	*1*	*5.141E+005*	*82.93*	*< 0.0001*	
C^2	*34688.47*	*1*	*34688.47*	*5.60*	*0.0294*	
D^2	*3.405E+005*	*1*	*3.405E+005*	*54.92*	*< 0.0001*	
Residual	1.116E+005	18	6198.95			
Cor Total	9.050E+006	24				

Std. Dev.	78.73	R-Squared	0.9877
Mean	764.88	Adj R-Squared	0.9836
C.V. %	10.29	Pred R-Square	0.9535
PRESS	4.211E+005	Adeq Precisior	50.046

Figure A.3: ANOVA statistics for R parametric model.

ANOVA for Response Surface Reduced Quadratic Model

Analysis of variance table [Partial sum of squares - Type III]

Source	Sum of Squares	df	Mean Square	F Value	p-value Prob > F	
Model	17.69	6	2.95	144.73	< 0.0001	significant
A-TWR	*1.350E-003*	*1*	*1.350E-003*	*0.066*	*0.7998*	
C-Clearance	*14.38*	*1*	*14.38*	*705.89*	*< 0.0001*	
D-Turns	*2.32*	*1*	*2.32*	*113.79*	*< 0.0001*	
CD	*0.66*	*1*	*0.66*	*32.60*	*< 0.0001*	
A^2	*0.096*	*1*	*0.096*	*4.73*	*0.0432*	
D^2	*0.14*	*1*	*0.14*	*6.81*	*0.0177*	
Residual	0.37	18	0.020			
Cor Total	18.06	24				

Std. Dev.	0.14	R-Squared	0.9797
Mean	8.17	Adj R-Squared	0.9729
C.V. %	1.75	Pred R-Square	0.9309
PRESS	1.25	Adeq Precisior	40.996

Figure A.4: ANOVA statistics for C_{inter} parametric model.

ANOVA for Response Surface Reduced Quadratic Model

Analysis of variance table [Partial sum of squares - Type III]

Source	Sum of Squares	df	Mean Square	F Value	p-value Prob > F	
Model	118.26	6	19.71	368.94	< 0.0001	significant
A-TWR	*0.060*	*1*	*0.060*	*1.12*	*0.3033*	
C-Clearance	*94.41*	*1*	*94.41*	*1767.06*	*< 0.0001*	
D-Turns	*20.91*	*1*	*20.91*	*391.32*	*< 0.0001*	
CD	*2.25*	*1*	*2.25*	*42.11*	*< 0.0001*	
A^2	*0.20*	*1*	*0.20*	*3.78*	*0.0677*	
D^2	*0.26*	*1*	*0.26*	*4.85*	*0.0408*	
Residual	0.96	18	0.053			
Cor Total	119.23	24				

Std. Dev.	0.23	R-Squared	0.9919
Mean	14.11	Adj R-Squared	0.9892
C.V. %	1.64	Pred R-Square	0.9753
PRESS	2.94	Adeq Precisior	64.864

Figure A.5: ANOVA statistics for C_{intra} parametric model.

Appendix B

Parametric Models: Interaction Plots

One of the most powerful capabilities of DoE methodology is the ability to identify interactions between factors. These are terms which are neglected in one-factor-at-a-time approaches [35]. The plots in this section compare the effect of one factor on a response at a low and high level of the term it interacts with. If the resulting curves are exactly parallel then there is no interaction between the two terms. The further the curves depart from being parallel the more significant the interaction. The most significant interactions in these models are between factor C (clearance) and factor D (number of turns per winding). This is intuitive considering both factors affect the total amount of copper used in the design, which has a direct effect on L_{lk}, R, C_{inter}, and C_{intra}.

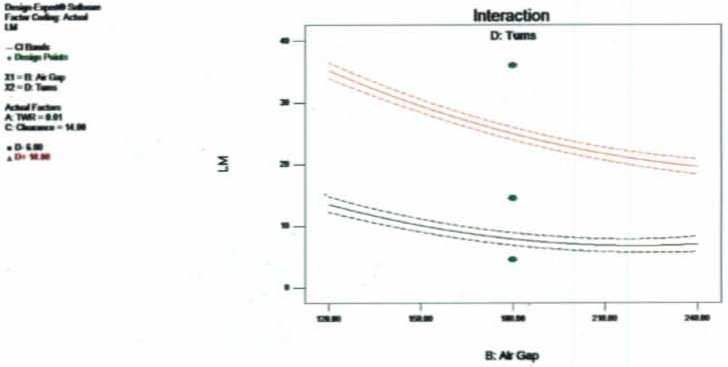

Figure B.1: The interaction between air gap and number of turns on L_M.

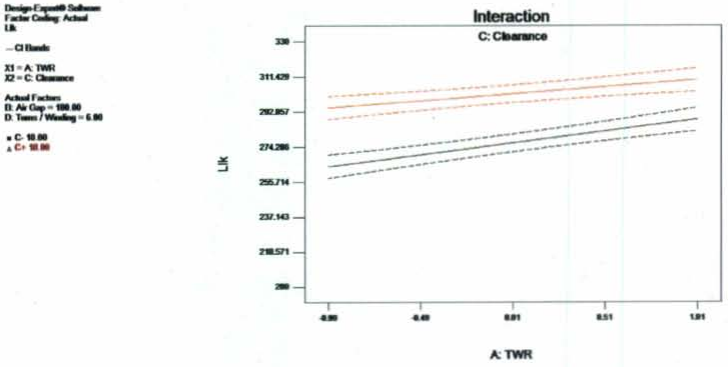

Figure B.2: The interaction between track width ratio and clearance on L_{lk}.

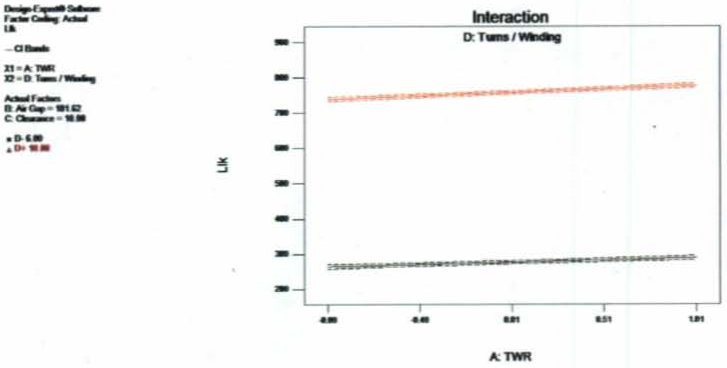

Figure B.3: The interaction between track width ratio and number of turns on L_{lk}.

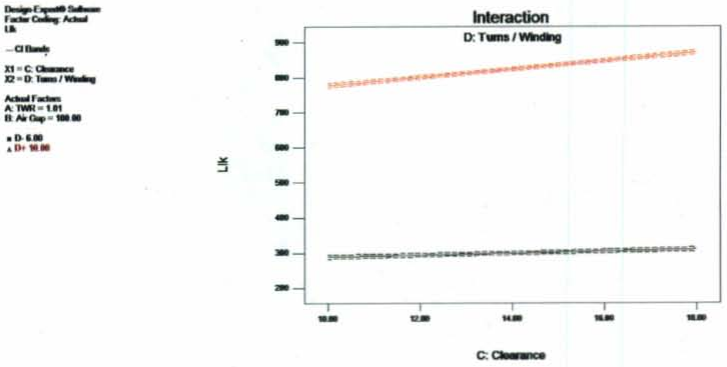

Figure B.4: The interaction between clearance and number of turns on L_{lk}.

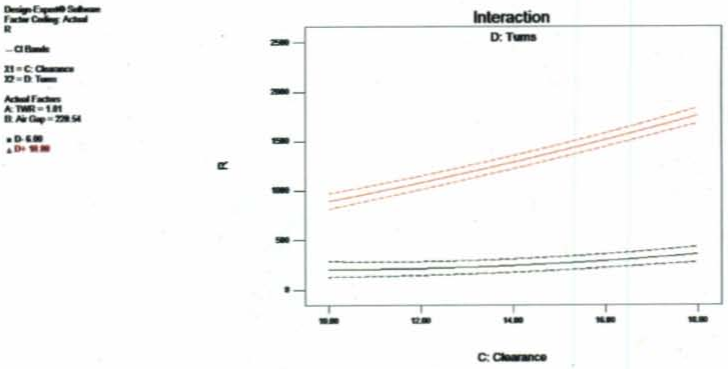

Figure B.5: The interaction between air gap and number of turns on R.

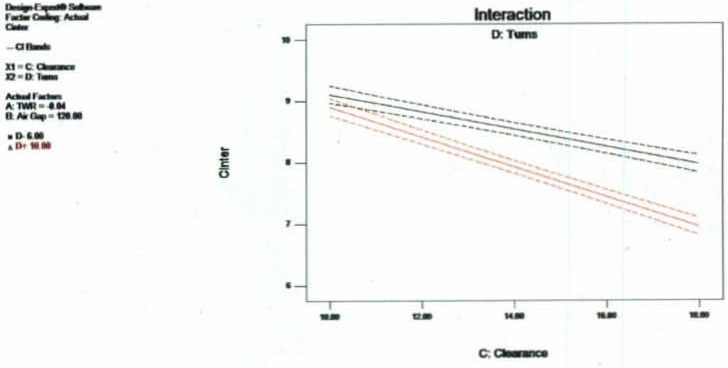

Figure B.6: The interaction between air gap and number of turns on C_{inter}.

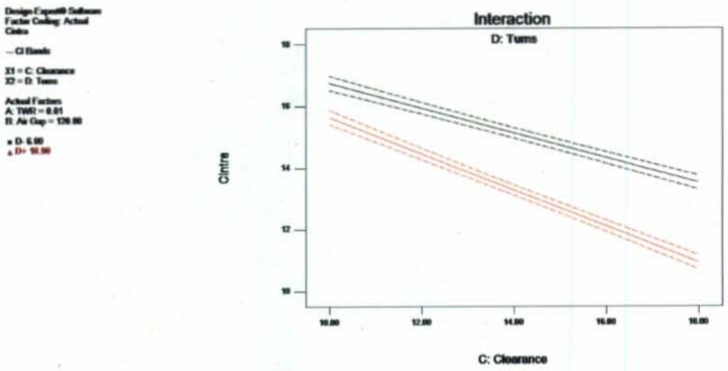

Figure B.7: The interaction between air gap and number of turns on C_{intra}.